Eng. Sci., 2025, **37**, 1714

Engineered Science
DOI: https://dx.doi.org/10.30919/es1714

Cellulose-based Ionic Conductive Hydrogels with Tunable Flexibility and Ionic Conductivity for Multifunctional Applications in Flexible Electronics

Ziqian Ye,[1,2] Yanshuo Yu,[2,3] Haiyue Miao,[2,4] Yiyang Liu,[5,6] Xiaojuan Huang,[7] Chongyang Zheng,[7] Xi Zhang,[8] Xiaobin Fu,[2] Jun Xu,[9] Hailong Huang,[2,*] Min Ge,[2] Yisheng Xu[1,*] and Yuan Qian[2,*]

Abstract

Wearable sensors and flexible energy storage devices impose distinct requirements on ionic conductive hydrogels, particularly regarding the balance between flexibility and conductivity. However, existing hydrogels lack a simple and scalable approach to tailor these properties for targeted applications, meeting the requirements of different applications. Here, we propose a strategy to regulate the microstructure of cellulose-based ionic conductive hydrogels (ICH) by leveraging competitive hydration effects between Zn^{2+} and Li^{+} ions, enabling single-step performance tuning. When Zn^{2+} dominates (ICH-1), hydrated ions expand cellulose chain spacing, enhancing ion mobility and yielding good conductivity (18.48 $mS{\cdot}cm^{-1}$). The resulting asymmetric flexible capacitor (ICH-1) achieves a 0-2.0 V voltage window, with exceptional energy density (50.6 $Wh{\cdot}kg^{-1}$) and power density (1000.1 $W{\cdot}kg^{-1}$). Conversely, Li^{+}-dominant ICH-3 exhibits compact cellulose chains, endowing good flexibility (311.84 kPa at 35% strain), ionic conductivity (13.16 $mS{\cdot}cm^{-1}$) and sensitive electromechanical performance (GF=2.78). This enables its application as a biomimetic e-skin sensor for real-time human motion monitoring and human-computer interaction. Our method addresses the limitations of conventional ICH fabrication, offering scalable production and demonstrating significant industrial potential.

Keywords: Cellulose hydrogel; Wearable sensor; Flexible supercapacitor; Molten salts hydrate; Flexible electronic devices.
Received: 10 June 2025; Revised: 16 August 2025; Accepted: 29 August 2025
Article type: Research article.

1. Introduction

Flexible electronic technology is evolving and reshaping modern lifestyles alongside advancements in science and technology.[1-3] Leveraging unique flexibility and extensibility, it demonstrates significant application potential across diverse domains,[4-7] including wearable devices, intelligent medical systems, consumer electronics, and aerospace.[8-14] Among advanced functional materials, ionic conductive hydrogels (ICHs) showed unique advantages and attractive prospects in flexible electronics due to their exceptional combination of electrical conductivity, mechanical flexibility, and biocompatibility.[15,16] In particular, biomass-derived variants (cellulose or chitosan systems) demonstrate sustainability benefits through renewable feedstocks and green processing compatibility. These remarkable properties position ICHs as promising candidates for next-generation flexible electronic devices.

Recently, bio-based ICHs have been widely employed in flexible electronic devices, showing remarkable development in wearable sensors and flexible energy storage devices. As flexible sensors, they could synchronously detect body movements and recognize motion direction for positive health detection through electromechanical responsiveness.[17,18] Additionally, they served as an electrolytes in flexible energy storage devices, maintaining excellent electrochemical performance and stability.[19,20]

However, existing ICHs struggle to reconcile conflicting performance metrics for dual applications as electrolytes and sensors.[21-23] When serving as electrolytes, ICHs require high ionic conductivity, good electrochemical performance, and wide working voltage range. To satisfy the requirements of

[1]*State Key Laboratory of Green Chemical Engineering and Industrial Catalysis, State Key Laboratory of Chemical Engineering, School of Chemical Engineering, East China University of Science and Technology, 130 Meilong Road, Shanghai, 200237, China*
[2]*State Key Laboratory of Thorium Energy, Shanghai Institute of Applied Physics, Chinese Academy of Science, 2019 Jialuo Road, Shanghai, 201800, China*
[3]*College of Science, Shenyang University of Chemical Technology, 11 11th Street, Shenyang, 110142, China*

flexible energy storage devices, it should also have some degree of flexibility.[24] But electrolyte-optimized designs often sacrifice stretchability to achieve high conductivity. Conversely, in order to satisfy the demands of electromechanical responsiveness, the hydrogel sensors demand good elasticity, flexibility, ionic conductivity, and stability to ensure reliable electromechanical responsiveness,[25] which typically compromise electrochemical stability under cyclic deformation. However, in order to improve the flexibility or conductivity of hydrogels respectively, different strategies or functional monomers are added.[26,27] There are limited methods that can independently control flexibility and conductivity solely by adjusting the composition ratio. Therefore, the key challenge lies in how to improve electrochemical performance for hydrogel electrolyte, while achieving an optimal balance between flexibility and ionic conductivity for hydrogel sensors through feasible method.

To address these problems, Wei *et al*.[28] designed a method to prepare the high-strength cellulosic hydrogels. Through solution annealing and dual cross-linking, the aggregation and crystallization of cellulosic hydrogels were improved, which could effectively enhance their mechanical properties. But the improving cross-linking density limited the ions migration. Zhang *et al*.[29] designed a polyelectrolyte-cellulose interpenetrating DN hydrogel and introduced lithium chloride to improve ionic conductivity, obtaining a hydrogel with high conductivity. This excessive focused on a single function not only limited the potential of conductive hydrogels in more diverse and complex application scenarios but also highlighted the serious challenges they face in preparation processes and large-scale production. Zhou *et al*.[30] reported a facile method to fabricate state-switchable cellulose hydrogels. Through Ca^{2+}/Zn^{2+} ion exchange after soaking in different solvents, the performance of the hydrogel was regulated. However, the unstable soaking preparation process hindered the development of cellulose hydrogels for flexible electronic devices. In addition, ion regulation strategies concerning nanofluidics, have emerged as an effective method, showing a unique selective ion-transport characteristics that make them applicable in energy harvesting and sensing.[31-33] However, due to high cost, processing complexity, and reliance on external power sources seriously limit its industrial development. Hence, to satisfy the needs of the hydrogel electrolyte and flexible sensor, a straightforward method for creating ionic conductive hydrogel with regulated performance must be developed. Unfortunately, little exploration has been reported until now.

In this work, we developed a green one-step synthesis of bio-based ICHs using a Zn^{2+}/Li^{+} hydrated molten salt solvent that directly converted raw cellulose into functional hydrogels. Leveraging the differential ionic radii, charge densities, and coordination behaviors of zinc and lithium ions with cellulose chains, the ionic conductivity and flexibility of cellulose hydrogel could be regulated by tuning the Zn^{2+}/Li^{+} ratio. This could meet the application of flexible energy storage devices and flexible sensors. In the Zn^{2+}/Li^{+} hydrated molten salt solvent system, Zn^{2+} dominated dissolution by forming stable coordination bonds with cellulose hydroxyls, disrupting hydrogen networks. While Li^{+} exhibited weaker coordination, promoting chain aggregation when dominant. Through adjusting Zn^{2+}/Li^{+} ratio controls hydrogel microstructure: Zn^{2+}-rich systems yield planar structures (enhanced conductivity), while Li^{+} promoted ordered networks (improved mechanical properties). This competitive coordination mechanism could effectively regulate the hydrogels performance. Based on these advantages, the ICH-1 exhibited good electrochemical performance in flexible supercapacitor. And, the ICH-3 demonstrated good flexibility and sensitive electromechanical performance as a wearable sensor. These advantages make the method have broad application prospects and important research value in the field of chemistry and materials science.

2. Experimental section

2.1 Materials

Cellulose (Mn = 8.0×10^5) was generously supplied by Wuhan University. Zinc chloride ($ZnCl_2$), lithium chloride (LiCl), N-methyl-2-pyrrolidone, Polyvinylidene fluoride (PVDF), carbon black (SP), and activated carbon (AC) were procured from Sinopharm Group. All the chemical reagents employed did not undergo further purification processes. For every experiment conducted in this study, deionized water was utilized.

2.2 Sample preparation

***Ionic conductive hydrogel (ICH)*:** A mixture of 17.86 g of $ZnCl_2$ and 7.14 g of LiCl was dissolved in 20 g of deionized water. The solution was heated to 90 °C and stirred at 600 rpm for 0.5 hours. 0.45 g of cellulose was added to the solution, which was then stirred at 1000 rpm for 2.0 hours until a homogeneous solution was obtained. To create the cellulose hydrogel, put the solution into the PTFE mold at ambient temperature to obtain ICH-1. To regulate the cellulose hydrogels properties, different compositions of $ZnCl_2$/LiCl solution were used in the preparation, as shown in Table S1.

***Carbon electrode*:** AC, PVDF, and SP were mixed according to the mass ratio of 8:1:1, and NMP was used as a

[4]*University of Chinese Academy of Sciences, Beijing, 100049, China*
[5]*Photon Science Research Center for Carbon Dioxide, Shanghai Advanced Research Institute, Chinese Academy of Sciences, Shanghai, 201210, China*
[6]*State Key Laboratory of Low Carbon Catalysis and Carbon Dioxide Utilization, Shanghai Advanced Research Institute, Chinese Academy of Sciences, Shanghai, 201210, China*
[7]*Department of Oral and Maxillofacial-Head & Neck Oncology, Shanghai Ninth People's Hospital, Shanghai Jiao Tong University School of Medicine, Shanghai, 200011, China*

solvent to disperse the mixture. Then a certain amount of slurry was sucked up with a rubber-tipped dropper and applied to the graphite paper (1×2 cm^2). After that, the coated graphite sheet was placed to dry to gain the carbon electrode.[34]

***Assembled asymmetric supercapacitor*:** ICH-1 hydrogel electrolyte, carbon electrode, and Zn foil were assembled into an asymmetric supercapacitor (ICH-1-ZHS) with a conventional sandwich structure for the electrochemical performance research.[35] Tests performed at 25°C/35% RH (encapsulated with polyurethane (PU) tape).

2.3 Characterization

Scanning electron microscopy (SEM, LEO 1530 VP) was employed to observe the morphology of both raw cellulose and ICHs. The chemical structures of cellulose hydrogels were investigated by X-ray diffraction (XRD, D8 Advance). Fourier transform infrared spectroscopy (FTIR, PerkinElmer spectrometer) was utilized to characterize the chemical structures of these materials. Differential scanning calorimetry (DSC) measurements were made using a Discovery DSC250 (TA Instruments, USA) under a nitrogen atmosphere.

2.4 Mechanical properties

The mechanical tensiometer (MARK-10 F105 IM) equipped with a 50 N load cell was employed to assess the tensile and compressive characteristics of ICHs. The hydrogels were stretched to a 20% strain continuously for 300 cycles without any breaks in order to perform a cyclic test. Additionally, the hydrogels were stretched to different strains without breaks in order to perform an energy dissipation test. The gradient of the tensile strain curve was used to get the elastic modulus (E). In the meantime, the area of the integral curve between the stress-strain curves was used to assess toughness. The dissipated energy (Uhys) was computed using the enclosed area of the integral curve between the loading and unloading curves.

2.5 Electrochemical performance

The electrochemical performance of the as-prepared ICH-1-ZHS, including cyclic voltammogram (CV), galvanostatic charging/discharging (GCD), and long-term stability tests, was performed by a commercial electrochemical workstation (CHI660E, China).

The conductivity of ICHs was measured through electrochemical impedance spectroscopy (EIS) and calculated according to Eq. (1),[36]

$$\sigma = \frac{L}{R \times S} \tag{1}$$

where R is the resistance, L is the length, and S is the cross-sectional area of the hydrogel.

Using the charge and discharge curves with constant current, the specific capacitance (C, $F \cdot g^{-1}$), energy density (E, $Wh \cdot kg^{-1}$), and power density (P, $W \cdot kg^{-1}$) may be calculated.

The specific capacitance (C, $F \cdot g^{-1}$) was calculated according to Eq. (2),[36]

$$C = \frac{I\Delta t}{m\Delta V} \tag{2}$$

where m (g) is the mass of the active material loaded by the supercapacitor electrode, Δt (s) is the discharge process time, I (A) is the current intensity during the discharge process, and ΔV (V) is the voltage during the discharge process.

The specific values of energy density (E, $Wh \cdot kg^{-1}$) and power density (P, $W \cdot kg^{-1}$) were calculated according to Eq. (3) and Eq. (4),[36]

$$E = \frac{C(\Delta V)^2}{2 \times 3600} \tag{3}$$

$$P = \frac{E}{\Delta t} \times 3600 \tag{4}$$

The coulomb efficiency can be obtained by calculating the discharge capacity and charging capacity, respectively, and calculating their ratios.

2.6 Electromechanical performance

Relative resistance changes (RRC) were used to evaluate the electromechanical performance of ICH-3.The RRC was calculated according to Eq. (5),[37]

$$RRC = \frac{\Delta R}{R_0} = \frac{R - R_0}{R_0} \times 100\% \tag{5}$$

where R_0 is the original resistance. R *is* the real-time resistance, respectively.

The gauge factor (GF) was measured according to Eq. (6),[37]

$$GF = \frac{\Delta R}{\varepsilon R_0} = \frac{R - R_0}{\varepsilon R_0} \tag{6}$$

where R_0 is the resistance in the original state and R is the resistance in the deformed state, respectively. ε is the applied strain to the hydrogel.

2.7 Wearable sensor

The ICH-3 wearable sensor tracked physiological signs and human body movements. In this application, the hydrogel was coupled with a wireless transmission module (ESP8266 Wi-Fi device) to create a comprehensive physiological signal detection platform. The wireless data acquisition system adopted a custom-designed circuit configuration, establishing a stable connection with a smartphone terminal via Wi-Fi

[8]*Public Technology Service Center, Shanghai Institute of Organic Chemistry, Chinese Academy of Sciences, Shanghai, 200062, China*
[9]*Large Industrial Reactor Engineering Research Center of Ministry of Education, School of Chemical Engineering, East China University of Science and Technology, 130 Meilong Road, Shanghai, 200237, China*
[*]*Email*: huanghailong@sinap.ac.cn (H. Huang),
yshxu@ecust.edu.cn (Y. Xu),
qianyuan@sinap.ac.cn (Y. Qian)

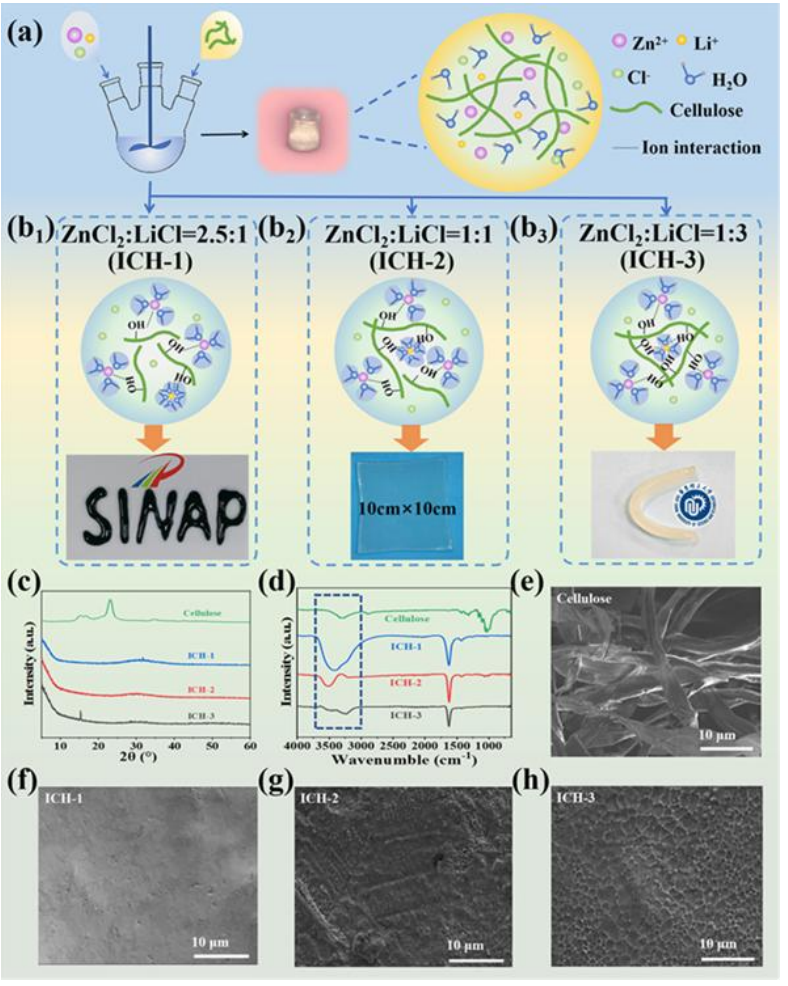

Fig. 1: Preparation and characterization of the ICHs. Schematics illustrating the preparation processes (a) and mechanism (b) of ICHs. XRD (c) and FTIR (d) spectra of raw cellulose and ICHs. (e-h) SEM images of raw cellulose and ICHs.

communication protocols. During operation, the hydrogel sensor was first electrically connected to the signal processing circuit. Subsequently, the integrated data acquisition subsystem continuously monitored and recorded electrical parameters (such as current and voltage variations) in real-time. These electrical signals, which corresponded to various physiological activities and body movements, were then wirelessly transmitted to the mobile application interface for visualization and further analysis. The wearable devices utilized wireless Wi-Fi to directly record and transfer the electronic signals. Medical-grade insulating tape was used to firmly attach the hydrogel sensor to body joints in order to ensure robust electrical connections during the motion tracking procedure. This setup allowed for the continuous measurement of resistance variations corresponding to specific movements through a Wi-Fi enabled data acquisition system operating at a 0.1 V working voltage. The wireless wearable device could detect human body movements (finger, wrist, and knee), physiological signals (plantar pressure), and human - computer interaction (different gestures, objects of different sizes and weights).

3. Results and discussion

3.1 Preparation of cellulose hydrogels

To address the requirements of different applications, a feasible strategy was designed for preparing cellulose-based ICHs with tunable performances in one step. $ZnCl_2$/LiCl aqueous solution was used as a dissolving medium to dissolve unprocessed cellulose and regenerate cellulose hydrogels (Fig. 1a). The cellulose hydrogel performance was controlled by regulating the ratio of Zn^{2+} and Li^+ in the solvent. When Zn^{2+} was dominant, hydrated Zn^{2+} ions could interact with hydroxyl groups on cellulose, expanding the cellulose chain distances. It was conducive to the ion migration in the frame of cellulose hydrogel to improve its electronic performance. Although the reduction of crosslinking density decreased the mechanical properties, it still could meet the application needs of hydrogel electrolytes. As shown in Fig. $1b_1$, to directly exhibit the flexibility of ICH-1, the hydrogel was dyed dark green. The ICH-1 demonstrated good plasticity and was prepared with different shapes by squeezing the syringe. When Zn^{2+}/Li^+ was in equilibrium, the hydrogel was equipped with good ionic conductivity and mechanical properties. The ICH-2 hydrogel could be used for large-size sample preparation (Fig. $1b_2$). When Li^+ was dominant, the hydration interaction of Li^+ ions with water molecules caused the hydrogel framework to

spatially condense, thus improving the strength of the ICH-3. In addition, the existing Li^+ ions could give the ICH-3 good ionic conductivity. The ICH-3 exhibited good flexibility and elasticity, as shown in Fig. 1b$_3$. By changing the proportion of metal ions in the solvent, the properties of cellulose hydrogels could be effectively regulated to achieve a one-step method to prepare ionic conductive hydrogels that meet different functional requirements.

XRD and FTIR were performed to study the chemical structure changes of raw cellulose and ICHs. As shown in Fig. 1c, the raw cellulose displayed three characteristic peaks. A prominent peak at 23.1° was associated with the (200) crystal face of cellulose I crystals. Meanwhile, the peaks at 15.3°and 16.8°were related to the (1-10) and (110) crystal faces of cellulose I crystals, respectively.[38] Compared with raw cellulose, there were no cellulose characteristic peaks in the ICHs pattern, indicating the good dissolution performance of Zn^{2+}/Li^+ hydrated molten salt system. Meanwhile, the broad peaks indicated that the ICHs frame structure was disordered, which would be conducive to maintaining stable flexibility of hydrogels. FTIR spectra further proved the chemical structure changes of ICHs by the Zn^{2+}/Li^+ hydrated molten salt system (Fig. 1d). The major functional groups of cellulose were displayed at 3333 cm^{-1} and 3334 cm^{-1}, 2895 cm^{-1}, 1110 cm^{-1}, and 1053 cm^{-1} due to the stretching vibrations of -OH, -CH_2, and -C-O-C-, respectively. The characteristic peaks at 1427 cm^{-1} and 898 cm^{-1} belonged to the -CH_2 bending stretching vibration and β-glycosidic bond between sugar units, respectively. Among them, the wide absorption band of hydrogel at 3235 cm^{-1} shows that the -OH group in cellulose forms hydrogen bonds with hydrated metal ions. The characteristic absorption peaks of hydrogel at 1615 cm^{-1} and 1490 cm^{-1} correspond to the stretching vibration of C=O. Different from raw cellulose, the stretching vibration peak of -OH in the hydrogel shifts toward lower wavenumbers and broadens. It can be attributed to the addition of hydrated metal ions, which promote coordination interactions between -OH groups and metal ions while breaking the initial hydrogen bonds between cellulose molecular chains.[39,40] Due to the varying content of hydrated ions in ICHs, the -OH peaks exhibited significant differential changes. With the increase in hydrated ions, the number of disrupted hydrogen bonds increased, leading to a reduction in the intensity of the broad -OH peak. Furthermore, microscopic morphology analysis revealed that the hydrated molten salt solvent could not only dissolve cellulose and regenerate cellulose hydrogel, but also regulate the cellulose microstructure (Fig. 1e-h). When zinc ions dominated, the microstructure of the ICH-1 hydrogel showed relative smoothness, indicating that zinc ions dissolved and dispersed the cellulose molecular chains. In contrast, when lithium ions dominated, the ICH-3 hydrogel demonstrated a dense structure (Fig. 1h), suggesting that lithium ions promote the aggregation of molecular chains. This trend was further confirmed by energy-dispersive X-ray spectroscopy (EDS) mapping (Fig. S1a-c).

3.2 Mechanical properties, conductivity, and stability of ICHs

In contrast to conventional cellulose solvents, the $ZnCl_2$/LiCl hydrated salt solvent was able to dissolve cellulose and create cellulose hydrogel in one step, while imparting favorable mechanical and ionic conductivity properties. Meanwhile, the performance could be regulated through adjusting the solvent composition without polymeric monomer or conductive additives. The mechanical properties improved as the lithium ion content increased, and the ICHs demonstrated good stress performance (Fig. 2a-b). Among the ICHs, the ICH-3 exhibited the best mechanical properties with 311.83 kPa at 35% compressive strain and 37.05 $kJ \cdot m^{-3}$ toughness, due to the hydrogel structure's spatial condensation brought on by the Li^+ ions' hydration process. The tensile stress-strain curves demonstrated the same trend (Fig. S2). Additionally, ICH-3 exhibited good elasticity (Fig. 2c-e). During the five continuous compression-release cycles, it maintained good mechanical elasticity and shape recovery ability, without any obvious structural deformation under distortion. Changes in the microstructure not only lead to regulating their mechanical properties, but also influenced the ionic conductivity. Fig. 2f-h showed the ionic conductivity of ICHs, due to the existing metal ions, the ICHs demonstrated good ionic conductivity. Compared with ICH-3 (15.91 $mS \cdot cm^{-1}$) and ICH-2 (13.16 $mS \cdot cm^{-1}$), the ICH-1 showed better conductivity (18.48 $mS \cdot cm^{-1}$). It should be attributed to the interactions between metal ions and cellulose molecules. When the solvent contained a high concentration of zinc ions, the ICH-1 hydrogel exhibited a flat structure. This structure was formed due to the strong interaction between the zinc ions and cellulose molecules, resulting in a higher concentration of freely mobile lithium ions. As the lithium ion content increased, excess lithium ions binded with cellulose molecules, reducing the number of freely mobile ions. Consequently, the conductivity of the ICH-2 hydrogel decreased. When the lithium ion content continued to increase, lithium ions were dominant. The hydration interaction of lithium ions with water molecules caused the hydrogel framework to spatially condense, thus improving the strength of the ICH-3. Meanwhile, the high concentration of lithium ions increased the number of freely mobile metal ions, thereby enhancing the conductivity of ICH-3. However, due to the increase in the aggregation of the structure, the mobility of Li^+ was restricted, resulting in no further improvement in ionic conductivity.

Besides, the ICHs showed good stability across a broad temperature range from -25 ℃ to 25 ℃ (Fig. 2i-j and Fig. S3). After 35 days, the water retention rate of ICH-1 was maintained above 86%, and the ionic conductivity was maintained above 90% at 25 ℃. Even at sub-zero temperature (-25 ℃), the water retention rate and ionic conductivity of ICH-1 remained stable without obvious decrease. It benefited from the $ZnCl_2$/LiCl hydrated salt solvent. The introduction of metal ions not only served as an additive component but also formed hydrated ions with water, effectively reducing the

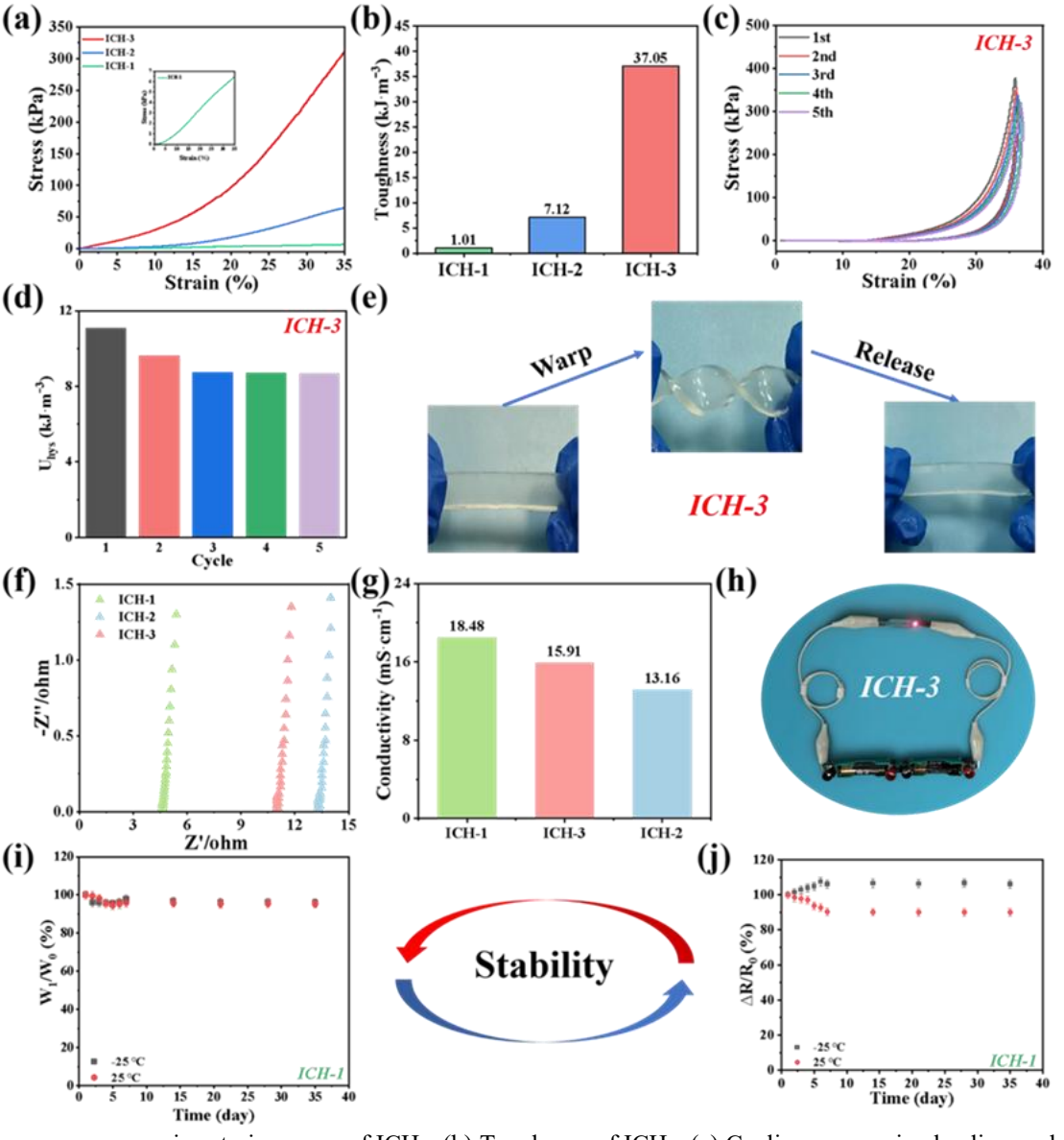

Fig. 2: (a) Compress–compressive strain curves of ICHs. (b) Toughness of ICHs. (c) Cyclic compressive loading–unloading curves of ICH-3 at strains of 35% for 5 cycles. (d) Dissipated energy of ICH-3 in the 5 cycles. (e) Photographs of ICH-3 undergoing warping and releasing. (f) EIS of ICHs. (g) Conductivities of ICHs. (h) Photograph illustrates the ICH-3 conductivity. (i) Changes in weight of ICH-1 of stored at -25 ℃ and 25 ℃ during 35 d. (j) RRC of ICH-1 of stored at -25 ℃ and 25 ℃ during 35 d.

saturated vapor pressure of water, thereby providing antifreeze and moisturizing effects (Fig. S4).[41]

3.3 Electrochemical performances of ICH-1 hydrogel

The conductivity and stability of the hydrogel electrolyte were critical to the electrochemical performance of energy storage devices. The better the conductivity and stability of the electrolyte, the better the electrochemical performance. Due to its good ionic conductivity, ICH-1 was used as the electrolyte to assemble an asymmetric flexible capacitor (ICH-1-ZHS) with zinc foil anode and AC cathode (Fig. 3a). The assembled ICH-1-ZHS showed good electrochemical performance. Only one ICH-1-ZHS could power the electronic watch for at least 7 days (Fig. 3b). Galvanostatic charge-discharge (GCD) and cyclic voltammetry (CV) was used to assess the electrochemical performance of ICH-1-ZHS.

As shown in Fig. 3c, across a broad working voltage span from 1.2 V to 2.0 V, the cyclic voltammetry (CV) curves of ICH-1-ZHS displayed a nearly rectangular shape. The CV curve could remain stable without polarization even at 2.0 V, indicating the wide and steady operating voltage range of ICH-1-ZHS. The galvanostatic charge-discharge (GCD) curves and capacitances of ICH-1-ZHS are shown in Fig. 3d-e for a variety of voltage windows (1.2 to 2.0 V). As the working voltage extended from 1.2 V to 2.0 V, the capacitance of ICH-1-ZHS notably increased from 80 $F \cdot g^{-1}$ to 105 $F \cdot g^{-1}$.The stability of ICH-1-ZHS was demonstrated using cyclic voltammetry (CV) curves at several sweep speeds (5, 20, 50, 70, and 100 $mV \cdot s^{-1}$) throughout a wide working voltage range of 0-2.0 V (Fig. 3f). It was observed that the CV curve displayed a symmetrical voltammogram with excellent

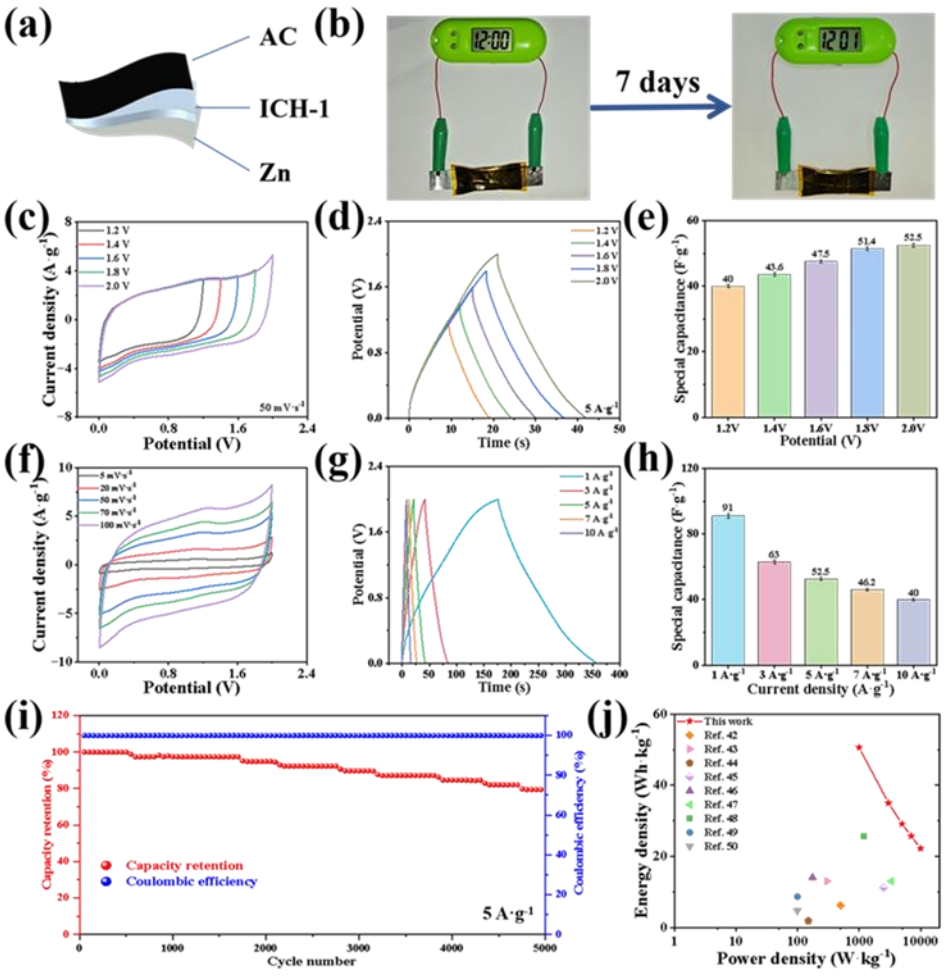

Fig. 3: Electrochemical performance of assembled ICH-1-ZHS. (a) Schematic of the ICH-1-ZHS. (b) Photographs of a lighted electronic watch powered by ICH-1-ZHS for 7 days. (c) CV curves at 50 $mV \cdot s^{-1}$ and (d) GCD curves at 5 $A \cdot g^{-1}$in different voltage windows. (e) Capacities in different voltage windows at 5 $A \cdot g^{-1}$. (f) CV curves at different scan rates and (g) GCD curves at various current densities in a working voltage range of 0–2.0 V. (h) Capacities at various current densities (1-10 $A \cdot g^{-1}$). (i) Cycling performance at the current density of 5 $A \cdot g^{-1}$. (j) Ragone plot Reproduced From.[42-50]

stability. Moreover, as the scanning rate rose, the curve did not deviate from the rectangular shape. Within the operating voltage range of 0-2.0 V, at different charging and discharging current densities between 1.0 and 10.0 $A \cdot g^{-1}$, the GCD curve of ICH-1-ZHS resembled an approximately symmetrical triangle. This indicates that ICH-1-ZHS possesses favorable capacitive properties and high charging efficiency (Fig. 3g). Additionally, in the working voltage range of 0-2.0 V, the corresponding specific capacitances of ICH-1-ZHS were 91 $F \cdot g^{-1}$, 63 $F \cdot g^{-1}$, 52.5 $F \cdot g^{-1}$, 46.2 $F \cdot g^{-1}$, and 40 $F \cdot g^{-1}$ at 1 $A \cdot g^{-1}$, 3 $A \cdot g^{-1}$, 5 $A \cdot g^{-1}$, 7 $A \cdot g^{-1}$, and 10 $A \cdot g^{-1}$ respectively (Fig. 3h). Furthermore, the assembled supercapacitor device demonstrated good cycling stability. The capacitance retention rate of the assembled capacitor declined gradually and eventually reached a stable state (Fig. 3i). The solid supercapacitor device demonstrated good stability for long-term operation with a capacitance retention rate of about 80% and a coulombic efficiency of about 100% after 5000 charge-discharge cycles. According to the Ragone plot (Fig. 3j), the developed SC's maximum energy and power densities (50.6 $Wh \cdot kg^{-1}$ and 1000.1 $W \cdot kg^{-1}$, respectively) were superior than those of the majority of hydrogel-based SCs that have been documented (Table 1). These electrochemical results highlighted the broad application prospects of the ICH-1-based SC in developing flexible energy-storage systems.

3.4 Electromechanical performance of ICH-3 hydrogel

Good flexibility and ionic conductivity could ensure the sensitive and stable electromechanical performance of hydrogel sensors. ICH-3 functioned as a versatile motion detection sensor as a result. ICH-3 exhibited good electromechanical responsiveness, capable of promptly responding to various deformations under both tensile and compressive states (Fig. 4a-b). Meanwhile, it showed sensitive electromechanical performance with a high GF of 2.78 in small strain. Even at different detection rates, it could maintain stable GF to accurately recognize the deformation (Fig. 4c). In addition, it demonstrated a high response rate, meeting detection requirements within the range of 0.004 Hz to 0.04 Hz (Fig. 4d). More importantly, due to the good freeze

Table 1: Summary of hydrogel electrolytes and supercapacitors.

Hydrogel	Voltage (V)	Specific Current ($A \cdot g^{-1}$)	Specific Capacitance ($F \cdot g^{-1}$)	Energy Density ($Wh \cdot kg^{-1}$)	Power Density ($W \cdot kg^{-1}$)	Temperature (°C)
SA/P(AA-AM)/NaCl[51]	1.4	0.8	27.7	7.41	560	25
P(AA-CO-AM)/Gel-g-GTA/FW SINCH[52]	2.0	2.0	191.6	21.04	2000	25
CN-15 wt% CHE[53]	1.8	0.2	34	7.65	90	25
Lig/SWCNT/$HrGO_{al}$[54]	1.0	1	249	8.65	125	25
PSCM/$ZnCl_2$[55]	2.0	1	242.8	137	1010	25
FZHSC[56]	1.8	—	53.18	47.86	580	25
poly(SBMA-co-HEAA)[57]	1.0	1	218.2	8.82	125	25
AF PVA-CMC/$Zn(CF_3SO_3)_2$[58]	1.8	0.25	242.8	87.9	162.8	25
PVA-SA[59]	1.5	0.0225	23.2	3.6	21.6	25
MSC[60]	1.0	0.2	30.98	11.45	250	25
This work	2.0	1.0	91	50.6	1000.1	25

resistance, the ICH-3 maintained good detection performance, even at sub-zero temperature (-25 °C) (Fig. 4e-f), indicating the good temperature tolerance of the ICH-3 sensor. In order to assess the stability of the hydrogel sensor, the ICH-3 was subjected to 300 cycles of stretching at 15% strain (Fig. 4h). The RRC was generally consistent without deformation or damage, indicating excellent repeatability and stability (Fig. 4g). In addition, the corresponding recovery time of the ICH-3 hydrogel was 0.2 s, which could meet the requirement of body motion detection (Fig. S5).[17] ICH-3 possessed precise detection capabilities, with a minimum detectable stress value of 0.5 N (Fig. 4i). Therefore, the ICH-3 hydrogels showed great potential and application value in sensing.

3.5 The application of ICH-3 hydrogel in wearable strain sensors

Based on the good electromechanical performance of ICH-3, a wearable sensor[61] was assembled with ICH-3, a Wi-Fi

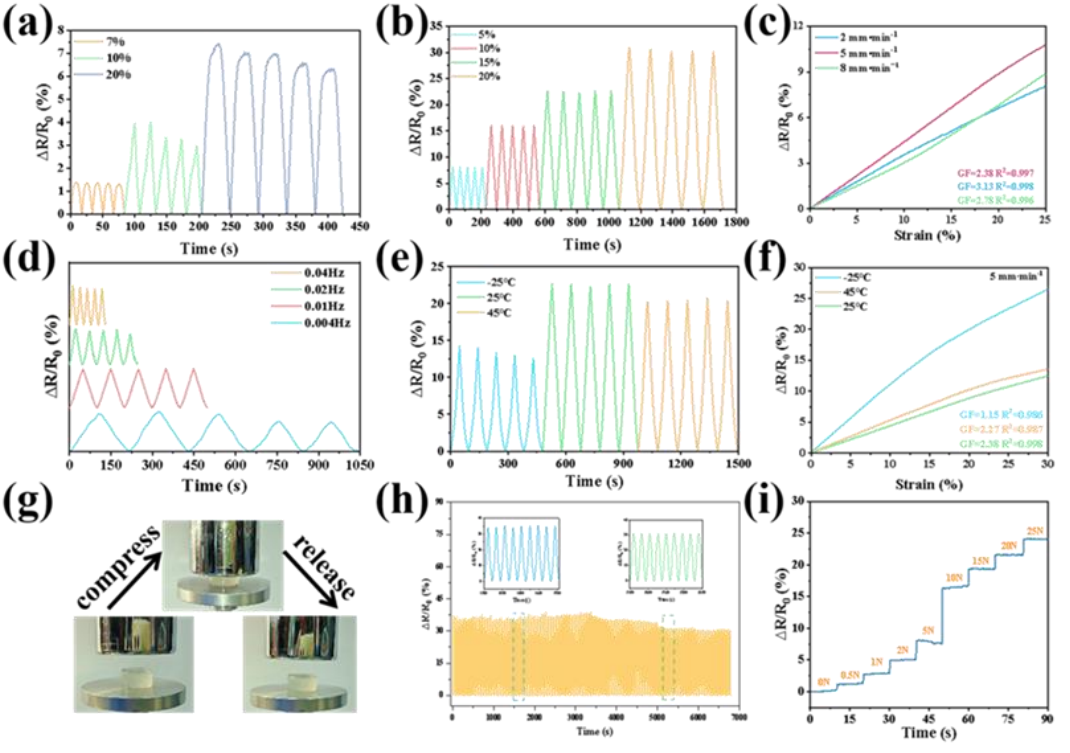

Fig. 4: Electromechanical performance of the ICH-3 hydrogel sensor. (a) Compressive strains curves. (b) Tensile strains curves. (c) RRC and the corresponding GF under various compressive rates. (d) Tensile rates curves at different frequencies. (e) RRC of ICH-3 hydrogel subjected to cyclic stretching at various tensile strains at different temperatures. (f) RRC and the corresponding GF under compression at different temperatures. (g) Photographs of the ICH-3 hydrogel undergoing compressing and releasing processes. (h) RRC of the ICH-3 hydrogel stretched for 300 cycles to a strain of 35% under stretching mode. (i) Compressive stresses curves at different forces.

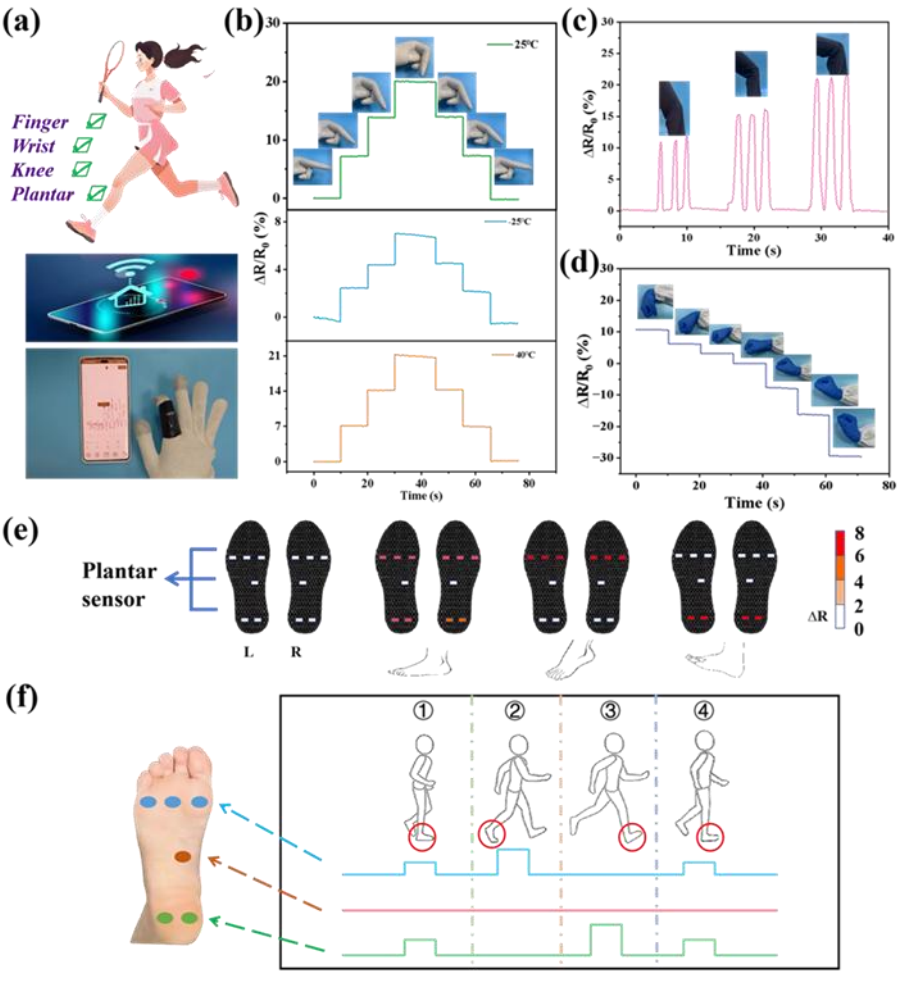

Fig. 5: (a) Illustration of wearable wireless sensor (ICH-3). (b) Finger motion detection under different bending angles from 0° to 90° at different temperatures (25 °C, -25 °C, and 40 °C). (c) Knee motion detection at different bending angles. (d) RRC to the wrist motion detection at different directions and bending angels. (e) Illustration of plantar pressure detection devices. (f) plantar pressure detection during the walking processes.

electric device, and a wearable pad to detect movements of the human body (Fig. 5a). It could be combined with Bluetooth technology and smartphone applications (apps) to demonstrate the motion detection data in real time (Movie S1-S2). To track point finger motions, the ICH-3 sensor was incorporated into the finger pads, shown in Fig. 5b. During the continuous bending and recovering processes of the point finger, the ICH-3 hydrogel sensor displayed excellent identification performance in real-time. The RRC can sensitively respond to and record electronic signals corresponding to different bending angles. Through the amplitude, cycles, and frequency of RRC signals, it could directly and easily recognize the finger motions' angle, times, and speed. More significantly, the ICH-3 sensor demonstrated outstanding detection performance by taking advantage of the good stability of ICH-track the plantar pressure and gait patterns for the purpose of disease prevention. A plantar detection apparatus, composed of six sensors embedded within the insole, was capable of documenting the distribution of plantar pressure across different foot regions, namely the forefoot, arch, and heel. The degree of color change corresponded to the level of pressure, 3 hydrogel throughout a broad operating temperature range, even at sub-zero temperature (-25 °C) and high temperature (40 °C). Fig. 5c showed the RRC of leg movements, indicating good detection performance. Besides, the ICH-3 demonstrated advantages in motion direction recognition. For example, as the wrist was bent downward, the corresponding RRC was a positive signal. While the wrist was bent upward, the corresponding RRC was a negative signal (Fig. 5d).

Plantar pressure and gait were critical parameters for measuring daily physiological information of the human body, which could assist physicians in diagnosing common foot diseases such as diabetic foot and foot trauma.[62] By capitalizing on the favorable electromechanical attributes of ionic conductive hydrogel, a pliable ICH - 3 hydrogel sensor was incorporated into an insole. This integration aimed to offering a straightforward way to comprehend the dynamic shifts in plantar pressure.[63] Take plantar pressure monitoring of the different gaits as an example (Fig. 5e). When a person is standing, the entire foot makes contact with the ground. At this time, the pressure is dispersed across the forefoot and the sole, while the arch experiences no pressure. When moving

forward, the forefoot touches the ground first, and the associated pressure is concentrated on the forefoot. Conversely, when the sole comes into contact with the ground, the pressure is distributed over the sole. As shown in Fig. 5f, using the monitoring of the right - foot's plantar pressure as an instance, the plantar pressure distribution changes with variations in gait and posture during normal walking. In addition to identifying the pressure characteristics of the human body under various physiological conditions, an analysis of the magnitude and distribution of plantar pressure can provide more useful guidance for functional rehabilitation, treatment effectiveness evaluation, and postoperative evaluation of foot-related disorders.

3.6 The application of ICH-3 hydrogel in human-computer interaction

Wearable electronics have been used increasingly developed in the field of human-computer interaction, which has greatly enhanced human-machine communication and enhanced machines' comprehension and responsiveness to human behavior.[64-66] The flexible sensor served as the bridge to connect human activity and machines. It could collect the human body movement and transmit the corresponding electronic signals to the machine, thus completing the human-machine synchronous control, which could endow the robot with human behavior and perception. Based on the sensing performance, the ICH-3 sensor could be used as the electronic skin to provide the sensing data for the smart hand control system. Fig. 6a showed the assembled ICH-3 sensor devices. Five ICH-3 sensors (10×10×2 mm^3) were fixed on the fingertip regions of each finger to monitor the touch stress of the fingers. And four identical sensors were fixed at the knuckles of fingers to detect gesture changes. This dual-sensor configuration enables comprehensive tactile perception and motion recognition of the hand for the smart machine hand control.

ICH-3 hydrogel sensor devices' performance was assessed using object gripping tests with varying gestures, dimensions, and masses (Fig. 6b-e). When catching an object, the changes in gestures and touch were detected by the hydrogel sensor and fed back in the form of electrical signals in real time. Fig. 6b exhibited holding a beaker with different fingers. When using the thumb and index finger to hold the beaker (Fig. $6b_1$), the stress was greater, and the curvature of the index finger was more significant. After adding the middle finger (Fig. $6b_2$) and the ring finger (Fig. $6b_3$), due to the participation of other fingers causing the pressure dispersion, the curvature and pressure of each finger were relatively reduced. When holding

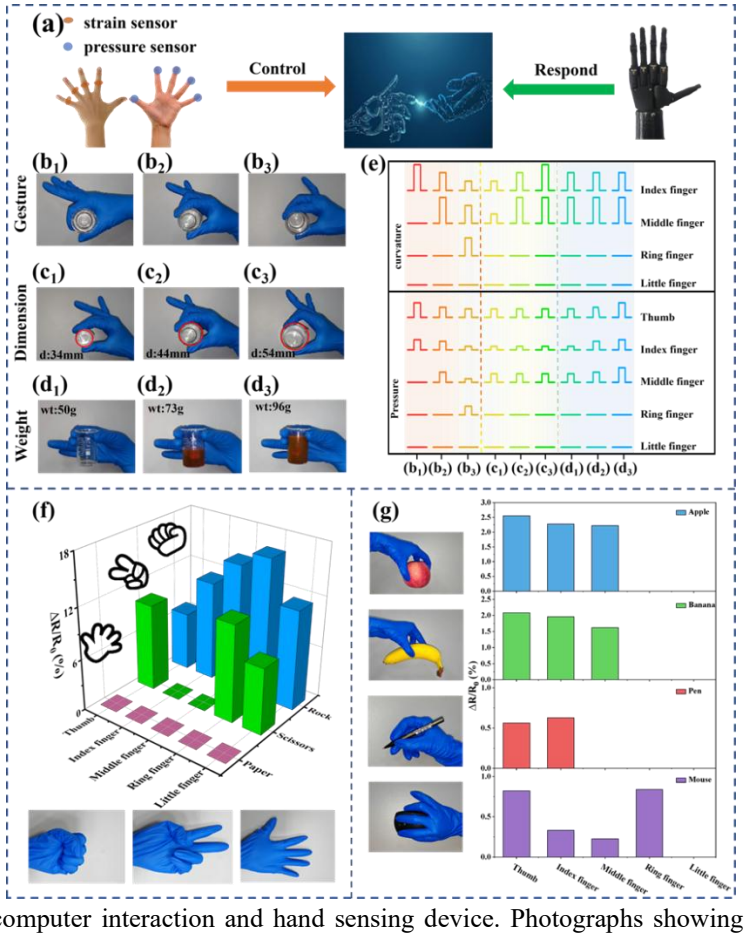

Fig. 6: (a) Diagram of human-computer interaction and hand sensing device. Photographs showing the use of human-computer interaction in gestures recognition (b), dimensions recognition (c), and weights recognition (d). (e) The corresponding RRC for the human-computer interaction application. (f) RRC and photographs to the rock-paper-scissors gesture. (g) The application of human-computer interaction for objects recognition.

a beaker of different dimensions (Fig. 6c) and masses (Fig. 6d) with fixed gestures, the finger flexion angles demonstrated size-dependent variations while the stress values demonstrated mass-dependent responses. Quantitative analysis of finger gesture and pressure enabled inverse determination of both object dimensions and weight. Through the hydrogel strain sensor, these subtle changes of the hand could be accurately captured and converted into electrical signals, providing original data support for the smart machine hand control system.

Taking advantage of hydrogel sensors in gesture detection and tactile perception, we explored the gesture interaction and object recognition experiments. Such as rock-paper-scissors (Fig. 6f), different gestures corresponded to different finger-bending changes, and then the gestures could be recognized and defined by RRC electrical signals. For example, the scissors gesture exhibited that the RRC were 10%, 11%, and 8% in the bending thumb, ring, and little fingers, respectively, while no signal was observed in the index and middle fingers. Besides, object recognition, such as apple, banana, pen, and mouse, could be identified based on the variations of pressure and gestures (Fig. 6g), which showed potential application scenarios in the field of human-computer interaction.

4. Conclusion

In this research, a method of dissolving cellulose with the $ZnCl_2$/LiCl hydrated molten salt solvent system to obtain ICH was proposed, which could meet the different functional requirements of different applications. ICH-1 hydrogel had good electrical conductivity and could be applied to flexible energy storage devices. Its operating voltage can reach 2.0 V, energy density can reach 50.6 $Wh \cdot kg^{-1}$, and power density can reach 1000.1 $W \cdot kg^{-1}$, which had significant performance advantages. ICH-3 hydrogel showed a good electromechanical response (GF=2.78) and could be used in sensors. It not only realized the detection of limb movement and physiological signals but also had potential application prospects in human-computer interaction. The ICH-3 sensor was equipped to detect a wide range of human motion signals when placed on diverse parts of the body, including the fingers, wrists, knees, and feet. In addition, a smart bionic hand sensor device detected the pressure and extension signals of different fingers. The outcomes of these experiments indicate that the sensor was well-suited for detecting the movement of humans, relaying information, identifying gestures, and multimodal detection. More importantly, this strategy greatly simplified the research and development process and shortens the product development cycle. The emergence of this technology not only promoted the rapid development of flexible electronics but also provided strong support for the realization of multifunctional, high-performance flexible electronic devices. In the future, with the in-depth research on the melting salt method to dissolve cellulose, we have reason to believe that more innovative applications based on this technology will continue to emerge, bringing a more intelligent and convenient way of life to human society.

Acknowledgments

This study was supported by the National Key Research and Development Program of China (2021YFB3500903), National Natural Science Foundation of China (No. 22273118, No. 82002853), the youth science and technology innovation of Shanghai Institute of Applied Physics, Chinese Academy of Science (SINAP-KJZX-202403), and Flexible hydrogel electrolyte performance and preparation process optimization research and development project (1124000525). 2023 Excellent Research Physician Training Program of Shanghai Ninth People's Hospital (2023yxyjxys-zcy).

The tests of the detecting device on human body (approved by Institutional Review Board of Shanghai Ninth People's Hospital, Shanghai Jiao Tong University School of Medicine Ethnics Committee (NO. SH9H-2021-T452-1)) do not affect living people physically or physiologically, and the authors did not seek or receive identifiable private information. The body shown in Figs. 5 and 6 are those of Z. Q. Ye (the first author), who gave consent for these images to appear here.

Conflict of Interest

The authors declare no conflict of interest.

Supporting Information

Applicable.

CRediT Statement

Ziqian Ye: Conceptualization, Methodology, Software, Investigation, Formal Analysis, Writing-Original Draft. **Yanshuo Yu, Haiyue Miao, and Yiyang Liu:** Methodology, Investigation, Data curation. **Xiaojuan Huang, Chongyang Zheng, and Xi Zhang:** Validation, Software, Formal analysis. **Xiaobin Fu, Jun Xu, and Min Ge:** Visualization. **Xiaobin Fu, Hailong Huang, and Yuan Qian:** Funding acquisition. **Hailong Huang, Yisheng Xu, and Yuan Qian:** Project administration, Supervision, Resources, Writing-review and editing. All authors reviewed the data and analysis, provided input on the manuscript, and approved the submission.

References

[1] J. He, L. Cao, J. Cui, G. Fu, R. Jiang, X. Xu, C. Guan, Flexible energy storage devices to power the future, *Advanced Materials*, 2024, **36**, e2306090, doi: 10.1002/adma.202306090.

[2] J.-H. Lee, K. Cho, J.-K. Kim, Age of flexible electronics: emerging trends in soft multifunctional sensors, *Advanced Materials*, 2024, **36**, e2310505, doi: 10.1002/adma.202310505.

[3] C. Xu, K. Yang, G. Zhu, C. Ou, J. Jiang, E. Zhuravlev, Y. Zhang, Anti-freezing multifunctional conductive hydrogels: from structure design to flexible electronic devices, *Materials Chemistry Frontiers*, 2024, **8**, 381-403, doi: 10.1039/D3QM00902E.

[4] L. Hu, P. L. Chee, S. Sugiarto, Y. Yu, C. Shi, R. Yan, Z. Yao, X. Shi, J. Zhi, D. Kai, H.-D. Yu, W. Huang, Hydrogel-based

flexible electronics, *Advanced Materials*, 2023, **35**, 2205326, doi: 10.1002/adma.202205326.
[5] Z. Yan, S. Luo, Q. Li, Z. S. Wu, S. F. Liu, Recent advances in flexible wearable supercapacitors: properties, fabrication, and applications, *Advanced Science*, 2024, **11**, e2302172, doi: 10.1002/advs.202302172.
[6] W. Chen, J. Ma, D. Yu, N. Li, X. Ji, Transparent, super stretchable, freezing−tolerant, self−healing ionic conductive cellulose based eutectogel for multi−functional sensors, *International Journal of Biological Macromolecules*, 2024, **266**, 131129, doi: 10.1016/j.ijbiomac.2024.131129.
[7] X.-L. Shi, L. Wang, W. Lyu, T. Cao, W. Chen, B. Hu, Z.-G. Chen, Advancing flexible thermoelectrics for integrated electronics, *Chemical Society Reviews*, 2024, **53**, 9254-9305, doi: 10.1039/D4CS00361F.
[8] S. Duan, H. Zhang, L. Liu, Y. Lin, F. Zhao, P. Chen, S. Cao, K. Zhou, C. Gao, Z. Liu, Q. Shi, C. Lee, J. Wu, A comprehensive review on triboelectric sensors and AI-integrated systems, *Materials Today*, 2024, **80**, 450-480, doi: 10.1016/j.mattod.2024.08.013.
[9] S. Yu, Research on the application of flexible electronics technology in wearable devices, *World Journal of Engineering and Technology*, 2024, **12**, 1024-1033, doi: 10.4236/wjet.2024.124064.
[10] X. Meng, C. Cai, B. Luo, T. Liu, Y. Shao, S. Wang, S. Nie, Rational design of cellulosic triboelectric materials for self-powered wearable electronics, *Nano-Micro Letters*, 2023, **15**, 124, doi: 10.1007/s40820-023-01094-6.
[11] Y. Cheng, Y. Xie, Z. Liu, S. Yan, Y. Ma, Y. Yue, J. Wang, Y. Gao, L. Li, Maximizing electron channels enabled by MXene aerogel for high-performance self-healable flexible electronic skin, *ACS Nano*, 2023, doi: 10.1021/acsnano.2c09933.
[12] D. Liu, C. Huyan, Z. Wang, Z. Guo, X. Zhang, H. Torun, D. Mulvihill, B. B. Xu, F. Chen, Conductive polymer based hydrogels and their application in wearable sensors: a review, *Materials Horizons*, 2023, **10**, 2800-2823, doi: 10.1039/D3MH00056G.
[13] H. Xu, G. Huang, H. Cheng, F. Li, Z. Zhang, X. Huang, H. Huang, C. Zheng, Thermoelectric-feedback nanocomposite hydrogel for temperature-synchronized monitoring and regulation in accurate photothermal therapy, *Advanced Healthcare Materials*, 2024, **13**, e2401609, doi: 10.1002/adhm.202401609.
[14] X. Pan, J. Li, N. Ma, X. Ma, M. Gao, Bacterial cellulose hydrogel for sensors, *Chemical Engineering Journal*, 2023, **461**, 142062, doi: 10.1016/j.cej.2023.142062.
[15] G. de Marzo, V. M. Mastronardi, M. T. Todaro, L. Blasi, V. Antonaci, L. Algieri, M. Scaraggi, M. De Vittorio, Sustainable electronic biomaterials for body-compliant devices: Challenges and perspectives for wearable bio-mechanical sensors and body energy harvesters, *Nano Energy*, 2024, **123**, 109336, doi: 10.1016/j.nanoen.2024.109336.
[16] Y. Zhang, Y. Tan, J. Lao, H. Gao, J. Yu, Hydrogels for flexible electronics, *ACS Nano*, 2023, **17**, 9681-9693, doi: 10.1021/acsnano.3c02897.
[17] G. Huang, H. Miao, X. Zhang, C. Zheng, X. Huang, Y. Liu, Y. He, X. Fu, M. Ge, H. Huang, R. Zhang, H. Liu, Y. Qian, A harsh environmental resistant and long-term stable ionic conductive hydrogel by one-step preparation for wireless health activity and physiological state detection, *International Journal of Biological Macromolecules*, 2024, **279**, 135286, doi: 10.1016/j.ijbiomac.2024.135286.
[18] F. Mo, P. Zhou, S. Lin, J. Zhong, Y. Wang, A review of conductive hydrogel-based wearable temperature sensors, *Advanced Healthcare Materials*, 2024, **13**(26), 2401503, doi: 10.1002/adhm.202401503.
[19] Y. Li, X. Wei, F. Jiang, Y. Wang, M. Xie, J. Peng, C. Yi, J. Li, M. Zhai, An ultrastretchable and highly conductive hydrogel electrolyte for all-in-one flexible supercapacitor with extreme tensile resistance, *Energy & Environmental Materials*, 2025, **8**, e12820, doi: 10.1002/eem2.12820.
[20] Z. Zhang, R. Zhang, Y. Gao, Y. Gao, F. Jia, G. Gao, Dendrite-free zinc anode enabled by zwitterionic organic hydrogel electrolytes for high-voltage zinc-ion hybrid capacitors, *Chemical Engineering Journal*, 2024, **484**, 149759, doi: 10.1016/j.cej.2024.149759.
[21] J. Chen, F. Liu, T. Abdiryim, X. Liu, An overview of conductive composite hydrogels for flexible electronic devices, *Advanced Composites and Hybrid Materials*, 2024, **7**, 35, doi: 10.1007/s42114-024-00841-6.
[22] J. Zhang, M. Zhang, H. Wan, J. Zhou, A. Lu, Coordinatively stiffen and toughen polymeric gels *via* the synergy of crystal-domain cross-linking and chelation cross-linking, *Nature Communications*, 2025, **16**, 320, doi: 10.1038/s41467-024-55245-3.
[23] H. Wan, Y. Chen, Y. Tao, P. Chen, S. Wang, X. Jiang, A. Lu, MXene-mediated cellulose conductive hydrogel with ultrastretchability and self-healing ability, *ACS Nano*, 2023, **17**, 20699-20710, doi: 10.1021/acsnano.3c08859.
[24] M. P. Chavhan, A. Kryeziu, S. Ganguly, J. Parmentier, Monolithic metal-based/porous carbon nanocomposites made from dissolved cellulose for use in electrochemical capacitor, *Green Carbon*, 2024, **2**, 109-117, doi: 10.1016/j.greenca.2024.01.001.
[25] Q. Li, B. Tian, J. Liang, W. Wu, Functional conductive hydrogels: from performance to flexible sensor applications, *Materials Chemistry Frontiers*, 2023, **7**, 2925-2957, doi: 10.1039/D3QM00109A.
[26] Q. Peng, J. Chen, T. Wang, X. Peng, J. Liu, X. Wang, J. Wang, H. Zeng, Recent advances in designing conductive hydrogels for flexible electronics, *InfoMat*, 2020, **2**, 843-865, doi: 10.1002/inf2.12113.
[27] T. Zhu, Y. Ni, G. M. Biesold, Y. Cheng, M. Ge, H. Li, J. Huang, Z. Lin, Y. Lai, Recent advances in conductive hydrogels: classifications, properties, and applications, *Chemical Society Reviews*, 2023, **52**, 473-509, doi: 10.1039/D2CS00173J.
[28] P. Wei, X. Yu, Y. Fang, L. Wang, H. Zhang, C. Zhu, J. Cai, Strong and tough cellulose hydrogels *via* solution annealing and dual cross-linking, *Small*, 2023, **19**, 2301204, doi: 10.1002/smll.202301204.

[29] R. Zhang, Z. Zhang, P. Xu, J. Xu, Y. Gao, G. Gao, Cellulose nanofiber hydrogel with high conductivity electrolytes for high voltage flexible supercapacitors, *Carbohydrate Polymers*, 2024, **326**, 121654, doi: 10.1016/j.carbpol.2023.121654.
[30] S. Zhou, K. Guo, D. Bukhvalov, X.-F. Zhang, W. Zhu, J. Yao, M. He, Cellulose hydrogels by reversible ion-exchange as flexible pressure sensors, *Advanced Materials Technologies*, 2020, **5**, 2000358, doi: 10.1002/admt.202000358.
[31] K. Yuan, A. A. University, Y. Shu, A. A. University, F. Chu, A. A. University, C. He, A. A. University, Z. Xiang, X. Fu, A. A. University, H. Wang, D. Ye, A. A. University, Microfluidic-mediated orientation nanoengineering for enhanced osmotic energy harvesting, *Nano Letters*, 2025, **25**, 8939-8947, doi: 10.1021/acs.nanolett.5c01019.
[32] Z. Lin, X. Fu, T. Yang, C. Jiao, K. Zheng, Q. Feng, S. Zhu, X. Zhou, Z. Liu, D. Ye, Customizable twisted nanofluidic cellulose fibers by asymmetric microfluidics for self-powered urine monitoring, *Advanced Functional Materials*, 2025, **35**, 2414365, doi: 10.1002/adfm.202414365.
[33] L. Zhang, A. A. University, Z. Yuan, A. A. University, X. Fu, A. A. University, S. Shi, A. A. University, X. Chen, A. A. University, P. Chen, D. Ye, A. A. University, Biomass-derived gradient and aligned structured aerogel for sustainable agricultural irrigation, *Nano Letters*, 2025, **25**, 5383-5390, doi: 10.1021/acs.nanolett.5c00520.
[34] Y. Zhou, H. Liu, X. Zhou, X. Lin, Y. Cai, M. Shen, X. Huang, H. Liu, X. Xu, Self-adhesive, freeze-tolerant, and strong hydrogel electrolyte containing xanthan gum enables the high-performance of zinc-ion hybrid supercapacitors, *International Journal of Biological Macromolecules*, 2024, **265**, 131143, doi: 10.1016/j.ijbiomac.2024.131143.
[35] Y. Tan, M. Xi, Y. Zhang, Z. Qiao, AA grafted PVA/CMC interpenetrating network gel polymer electrolyte for quasi-solid-state zinc ion hybrid supercapacitor, *Journal of Power Sources*, 2024, **624**, 235554, doi: 10.1016/j.jpowsour.2024.235554.
[36] K. Chen, J. Huang, J. Yuan, S. Qin, P. Huang, C. Wan, Y. You, Y. Guo, Q. Xu, H. Xie, Molecularly engineered cellulose hydrogel electrolyte for highly stable zinc ion hybrid capacitors, *Energy Storage Materials*, 2023, **63**, 102963, doi: 10.1016/j.ensm.2023.102963.
[37] H. Wanyan, Q. Li, H. Huang, J. Li, L. Huang, L. Chen, J. Wei, X. Zhou, Z. Tang, H. Wu, Flexible high electrochemical active hydrogel for wearable sensors and supercapacitor electrolytes, *International Journal of Biological Macromolecules*, 2024, **277**, 134356, doi: 10.1016/j.ijbiomac.2024.134356.
[38] X. Li, Y. Wang, Y. Tian, Z. Wang, L. Zhang, J. Ma, Aqueous $AlCl_3/ZnCl_2$ solution room-induced the self-growing strategy of expanded topological network for cellulose/polyacrylamide-based solid-state electrolytes, *Journal of Colloid and Interface Science*, 2024, **670**, 311-322, doi: 10.1016/j.jcis.2024.05.102.
[39] H. Miao, Y. Liu, C. Zheng, X. Huang, Y. Song, L. Tong, C. Dong, X. Fu, H. Huang, M. Ge, H. Liu, Y. Qian, A flexible, antifreezing, and long-term stable cellulose ionic conductive hydrogel *via* one-step preparation for flexible electronic sensors, *Carbohydrate Polymers*, 2025, **351**, 122936, doi: 10.1016/j.carbpol.2024.122936.
[40] W. Ma, X. Li, L. Zhang, Y. Zheng, Y. Xi, J. Ma, Z. Wang, Novel insights on room temperature-induced cellulose dissolution mechanism *via* $ZnCl_2$ aqueous solution: Migration, penetration, interaction, and dispersion, *International Journal of Biological Macromolecules*, 2024, **272**, 132912, doi: 10.1016/j.ijbiomac.2024.132912.
[41] M. Chen, Q. Quan, Z. You, Y. Dong, X. Zhou, Low-temperature strain-sensitive sensor based on cellulose-based ionic conductive hydrogels with moldable and self-healing properties, *International Journal of Biological Macromolecules*, 2023, **253**, 127396, doi: 10.1016/j.ijbiomac.2023.127396.
[42] N. Luo, J. Wang, D. Zhang, Y. Zhao, Y. Wei, Y. Liu, Y. Zhang, S. Han, X. Kong, P. Huo, Inorganic nanoparticle-enhanced double-network hydrogel electrolytes for supercapacitor with superior low-temperature adaptability, *Chemical Engineering Journal*, 2024, **479**, 147741, doi: 10.1016/j.cej.2023.147741.
[43] R. Elashnikov, O. Khrystonko, T. Jilková, S. Rimpelová, J. Prchal, I. Khalakhan, Z. Kolská, V. Švorčík, O. Lyutakov, High-strength self-healable supercapacitor based on supramolecular polymer hydrogel with upper critical solubility temperature, *Advanced Functional Materials*, 2024, **34**, 2314420, doi: 10.1002/adfm.202314420.
[44] Y. Zhao, Q. Liang, S. M. Mugo, L. An, Q. Zhang, Y. Lu, Self-healing and shape-editable wearable supercapacitors based on highly stretchable hydrogel electrolytes, *Advanced Science*, 2022, **9**, e2201039, doi: 10.1002/advs.202201039.
[45] Q. Wu, C. Jiang, S. Zhang, S. Yu, L. Huang, Self-assembly of biomass-based hybrid hydrogel electrode for an additive-free flexible supercapacitor, *Journal of Materials Chemistry A*, 2022, **10**, 16853-16865, doi: 10.1039/D2TA03710F.
[46] D. Guo, Z. Li, P. Liu, M. Sun, N, P, S Co-doped biomass-derived hierarchical porous carbon through simple phosphoric acid-assisted activation for high-performance electrochemical energy storage, *International Journal of Hydrogen Energy*, 2021, **46**, 8197-8209, doi: 10.1016/j.ijhydene.2020.12.013.
[47] G. Jung, H. Lee, H. Park, J. Kim, J. W. Kim, D. S. Kim, K. Keum, Y. H. Lee, J. S. Ha, Temperature-tolerant flexible supercapacitor integrated with a strain sensor using an organohydrogel for wearable electronics, *Chemical Engineering Journal*, 2022, **450**, 138379, doi: 10.1016/j.cej.2022.138379.
[48] D. Wang, Z. Li, L. Yang, J. Zhang, Y. Wei, Q. Feng, Q. Wei, Hydrogel electrolyte based on sodium polyacrylate/KOH hydrogel reinforced with bacterial cellulose aerogel for flexible supercapacitors, *Chemical Engineering Journal*, 2023, **454**, 140090, doi: 10.1016/j.cej.2022.140090.
[49] K. Zhang, Y. Pang, C. Chen, M. Wu, Y. Liu, S. Yu, L. Li, Z. Ji, J. Pang, Stretchable and conductive cellulose hydrogel electrolytes for flexible and foldable solid-state supercapacitors, *Carbohydrate Polymers*, 2022, **293**, 119673, doi: 10.1016/j.carbpol.2022.119673.
[50] S. Cui, W. Miao, X. Wang, K. Sun, H. Peng, G. Ma, Multifunctional zincophilic hydrogel electrolyte with abundant hydrogen bonds for zinc-ion capacitors and supercapacitors, *ACS Nano*, 2024, **18**, 12355-12366, doi: 10.1021/acsnano.4c01304.

[51] Z. Yang, L. Han, X. Fu, Y. Wang, H. Huang, M. Xu, Double-safety flexible supercapacitor basing on zwitterionic hydrogel: over-heat alarm and flame-retardant electrolyte, *Advanced Composites and Hybrid Materials*, 2022, **5**, 1876-1887, doi: 10.1007/s42114-022-00497-0.
[52] C. Gao, Z. Gao, Y. Wei, N. Luo, Y. Liu, P. Huo, Flexible wood enhanced poly (acrylic acid-co-acrylamide)/quaternized gelatin hydrogel electrolytes for high-energy-density supercapacitors, *ACS Applied Materials & Interfaces*, 2023, **15**, 2951-2960, doi: 10.1021/acsami.2c18935.
[53] S. Chen, J. Huang, H. Wang, X. Liu, G. Gao, X. Liu, Q. Zhang, Zincophilic zwitterionic hydrogel electrolyte towards dendrite-free zinc ion hybrid supercapacitors with anti-self-discharge ability, *Chemical Engineering Journal*, 2024, **501**, 157589, doi: 10.1016/j.cej.2024.157589.
[54] Z. Peng, C. Yu, W. Zhong, Facile preparation of a 3D porous aligned graphene-based wall network architecture by confined self-assembly with shape memory for artificial muscle, pressure sensor, and flexible supercapacitor, *ACS Applied Materials & Interfaces*, 2022, **14**, 17739-17753, doi: 10.1021/acsami.2c00987.
[55] R. Li, W. Jia, J. Wen, G. Hu, T. Tang, X. Li, L. Jiang, M. Li, H. Huang, G. Fang, MXene/zwitterionic hydrogel oriented anti-freezing and high-performance zinc–ion hybrid supercapacitor, *Advanced Functional Materials*, 2024, **34**, 2409207, doi: 10.1002/adfm.202409207.
[56] Y. Jiang, K. Ma, M. Sun, Y. Li, J. Liu, All-climate stretchable dendrite-free Zn-ion hybrid supercapacitors enabled by hydrogel electrolyte engineering, *Energy & Environmental Materials*, 2023, **6**, e12357, doi: 10.1002/eem2.12357.
[57] G. Zhang, X. Yang, H. Shu, W. Zhong, Ultrahigh conductivity and antifreezing zwitterionic sulfobetaine hydrogel electrolyte for low-temperature resistance flexible supercapacitors, *Journal of Materials Chemistry A*, 2023, **11**, 9097-9111, doi: 10.1039/D3TA00835E.
[58] X. Zhu, C. Ji, Q. Meng, H. Mi, Q. Yang, Z. Li, N. Yang, J. Qiu, Freeze-tolerant hydrogel electrolyte with high strength for stable operation of flexible zinc-ion hybrid supercapacitors, *Small*, 2022, **18**, e2200055, doi: 10.1002/smll.202200055.
[59] B. Huang, W. Liu, Y. Lan, Y. Huang, L. Fu, B. Lin, C. Xu, Highly ion-conducting, robust and environmentally stable poly(vinyl alcohol) eutectic gels designed by natural polyelectrolytes for flexible wearable sensors and supercapacitors, *Chemical Engineering Journal*, 2024, **480**, 147888, doi: 10.1016/j.cej.2023.147888.
[60] X. Yang, X. Cheng, S. Liao, D. Chen, Q. Wei, A self-healing and sweat-chargeable hydrogel electrolyte for all-in-one flexible supercapacitors, *ACS Applied Materials & Interfaces*, 2024, **16**, 49337-49348, doi: 10.1021/acsami.4c09054.
[61] Y. Wang, W. Jiang, Y. Yang, C. Wang, D. Zhao, X. Ji, Y. Liu, G. Yang, J. Chen, Y. Ni, G. Lyu, Ternary systems engineered conductive hydrogel with extraordinary strength, environmental adaptability and excellent electrochemical performances for flexible power supply devices, *Energy Storage Materials*, 2024, **70**, 103483, doi: 10.1016/j.ensm.2024.103483.
[62] W. Li, K. Zou, J. Guo, C. Zhang, J. Feng, J. You, G. Cheng, Q. Zhou, M. Kong, G. Li, C. F. Guo, J. Yang, Integrated fibrous iontronic pressure sensors with high sensitivity and reliability for human plantar pressure and gait analysis, *ACS Nano*, 2024, **18**, 14672-14684, doi: 10.1021/acsnano.4c02919.
[63] Z. Xiong, Y. Bai, L. Li, Z. Zhou, T. Li, T. Zhang, Rational design of a laminate-structured flexible sensor for human dynamic plantar pressure monitoring, *Microsystems & Nanoengineering*, 2024, **10**, 98, doi: 10.1038/s41378-024-00717-1.
[64] D. Boateng, X. Li, Y. Zhu, H. Zhang, M. Wu, J. Liu, Y. Kang, H. Zeng, L. Han, Recent advances in flexible hydrogel sensors: Enhancing data processing and machine learning for intelligent perception, *Biosensors and Bioelectronics*, 2024, **261**, 116499, doi: 10.1016/j.bios.2024.116499.
[65] Y. Fu, C. Yang, B. Zhang, Z. Wan, S. Wang, K. Zhang, L. Yang, R. Wei, A highly sensitive, conductive, and flexible hydrogel sponge as a discriminable multimodal sensor for deep-learning-assisted gesture language recognition, *Advanced Functional Materials*, 2025, **35**, 2416453, doi: 10.1002/adfm.202416453.
[66] T. Sun, B. Feng, J. Huo, Y. Xiao, W. Wang, J. Peng, Z. Li, C. Du, W. Wang, G. Zou, L. Liu, Artificial intelligence meets flexible sensors: emerging smart flexible sensing systems driven by machine learning and artificial synapses, *Nano-Micro Letters*, 2023, **16**, doi: 10.1007/s40820-023-01235-x.